Geochemistry Geophysics Geosystems G3

Published by AGU and the Geochemical Society

Article
Volume 14, Number 3
6 March 2013
doi:10.1002/ggge.20058
ISSN: 1525-2027

High density of structurally controlled, shallow to deep water fluid seep indicators imaged offshore Costa Rica

Jared W. Kluesner, Eli A. Silver, and James Gibson
Department of Earth and Planetary Sciences, University of California, Santa Cruz, California, USA (jwkluesne@ucsc.edu)

Nathan L. Bangs and Kirk D. McIntosh
Institute for Geophysics, University of Texas, Austin, Texas, USA

Daniel Orange
Niko Resources Ltd., Jakarta, Indonesia

Cesar R. Ranero
Barcelona Center for Subsurface Imaging, Instituto de Ciencias del Mar, ICREA at CSIC, Spain

Roland von Huene
University of California, Davis, California, USA

[1] We used high-resolution mapping to document 161 sites of potential fluid seepage on the shelf and slope regions where no geophysical seep indicators had been reported. Identified potential seabed seepage sites show both high-backscatter anomalies and bathymetric expressions, such as pockmarks, mounds, and ridges. Almost all identified seabed features are associated with bright spots and flat spots beneath, as mapped within the 3-D seismic grid. We obtained EM122 multi-beam data using closely spaced receiver beams and 4–5 times overlapping multi-beam swaths, which greatly improved the sounding density and geologic resolvability of the data. At least one location shows an acoustic plume in the water column on a 3.5 kHz profile, and this plume is located along a fault trace and above surface and subsurface seepage indicators. Fluid indicators are largely associated with folds and faults within the sediment section, and many of the faults continue into and offset the reflective basement. A dense pattern of normal faults is seen on the outer shelf in the multi-beam bathymetry, backscatter, and 3-D seismic data, and the majority of fluid seepage indicators lie along mapped fault traces. Furthermore, linear mounds, ridges, and pockmark chains are found on the upper, middle, and lower slope regions. The arcuate shape of the shelf edge, projection of the Quepos Ridge, and high density of potential seep sites suggest that this area may be a zone of former seamount/ridge subduction. These results demonstrate a much greater potential seep density and distribution than previously reported across the Costa Rican margin.

Components: 12,500 words, 15 figures.

Keywords: fluid seepage; fluid flow; subduction zones; Marine Geology and Geophysics; Costa Rica.

Index Terms: 3060 Marine Geology and Geophysics: Subduction zone processes (1031, 3613, 8170, 8413); 8045 Structural Geology: Role of Fluids; 3004 Gas and Hydrate Systems.

Received 28 August 2012; **Revised** 26 December 2012; **Accepted** 26 December 2012; **Published** 6 March 2013.

Kluesner J. W., E. A. Silver, N. L. Bangs, K. D. McIntosh, J. Gibson, D. Orange, C. R. Ranero, and R. von Huene (2013), High density of structurally controlled, shallow to deep water fluid seep indicators imaged offshore Costa Rica, *Geochem. Geophys. Geosys.*, *14*, 519–539, doi:10.1002/ggge.20058.

1. Introduction

[2] Geophysical fluid flow indications on the surface and subsurface regions of continental margins are significant for biological [*Kulm et al*., 1986; *Paull et al*., 1995], structural [*Hovland et al*., 2002], and seismological processes [*Field and Jennings*, 1987]. Fluid seepage is controlled in part by structural features such as faults (providing high permeability pathways) and folds (focusing flow and trapping fluids in pockets). Seismic shaking is considered responsible for generating out-gassing on active margins [*Field and Jennings*, 1987; *Judd and Hovland*, 2007]. Surface indicators of fluid and gas seepage include pockmarks [*Hovland et al*., 2002], acoustic signatures of gas [*Géli et al*., 2008], mud volcanoes, carbonate or mud mounds, often showing zones of high acoustic backscatter, and chemosynthetic fauna [*Sahling et al*., 2008]. Previous studies of the Central American continental margin have documented abundant fluid indicators, such as mud volcanoes [*Kahn et al*., 1996; *Grevemeyer et al*., 2004]. Synthesizing numerous fluid studies along the Central American margin, *Sahling et al*. [2008] and *Ranero et al*. [2008] proposed that most of the fluid indicators were from the mid-slope region, with very few from the lower or upper slope and none from the shelf.

[3] Accretionary margins might be expected to show higher rates of fluid and gas escape because of the continuing collapse of a thick pile of off-scraped trench sediments making up the accretionary wedge [*Moore and Saffer*, 2001]. However, numerous studies of the Central American erosional margin have shown a high amount of dewatering related to complete subduction of a thin, water-rich layer of incoming sediment [*Silver et al*., 2000], clay and silica dehydration at moderate depth [*Hensen et al*., 2004], and possibly from dewatering of serpentine at greater depths [*Tryon et al*., 2010]. A very high methane flux rate was measured on the Jaco Scar off Central Costa Rica [*Mau et al*., 2012]. Degassing of continental margins also plays a role in modulating the carbon budget of the atmosphere [*Hovland and Judd*, 1992; *Kvenvolden*, 1993; *Kvenvolden and Rogers*, 2005].

[4] Here we report on a detailed multi-beam and backscatter study carried out as part of a 3-D seismic experiment off southern Costa Rica [*Bangs et al*., 2011]. Because of the closely spaced ship tracks, we were able to collect the multi-beam data in narrow-fixed swath mode, providing very high across and along-track sounding density and significant data overlap, greatly improving the geologic resolvability of the data. These acquisition parameters allowed us to grid the bathymetry data and mosaic the backscatter data at very small cell sizes throughout the survey region. In addition, we are able to tie identified surface features with the subsurface structure using the 3-D seismic data. We find a high number (161) of surface and subsurface geophysical indicators of fluid flow and seepage in this 11 km × 55 km rectangular area, where previous studies using the standard wide-angle mode of multi-beam acquisition identified none. We also found evidence of an active gas plume on the shelf, extending to the sea surface.

[5] We first discuss the structure of the margin, with special emphasis on a dense array of normal faults marking the outer part of the continental shelf, a series of large folds running sub-parallel to the trench, and oblique faults cutting the upper and middle slope regions. We then discuss our evidence for numerous geophysical indicators of subsurface fluid flow and potential seafloor seepage throughout the margin, followed by a discussion of the potential significance of these findings for fluid pathways through the margin.

2. Background

[6] The Middle-America subduction zone has been studied by seismology [*Protti et al*., 1995; *Newman et al*., 2002; *Bilek et al*., 2003; *DeShon et al*., 2003], seismic reflection imagery [*Shipley et al*., 1992; *von Huene et al*., 2000; *Ranero et al*., 2008], wide angle refraction [*Ye et al*., 1996; *Christeson et al*., 2000], multi-beam bathymetry [*Ranero and von Huene*, 2000], submersible diving [*Kahn et al*., 1996; *McAdoo et al*., 1996], and scientific drilling [*Kimura et al*., 1997; *Morris et al*., 2003; *Vannucchi et al*., 2012]. One remarkable feature of the Pacific

margin of Costa Rica is the series of seamount tracks that can be mapped across the slope [*von Huene et al.*, 2000; *Ranero and von Huene*, 2000]. Seamount and ridge collision has played a significant role in the tectonics of Costa Rica [*Gardner et al.*, 1992; *Fisher et al.*, 1998; *Sitchler et al.*, 2007]. *Vannucchi et al.* [2001, 2003] showed convincing evidence for long-term subsidence, probably caused by subduction erosion along the Costa Rica margin, interpreting that the outer 50 km of material of the margin had been eroded away over the past 6.5 Ma offshore of Nicoya Peninsula. Very little subsidence (and presumably subduction erosion) occurred between 16.5 and 6.5 Ma.

[7] Based on ALVIN dives, *Kahn et al.* [1996] and *McAdoo et al.* [1996] documented evidence for active bioherms, indicating fluid expulsion on the Costa Rica margin seaward of the Nicoya Peninsula. Scientific drilling in this region [*Kimura et al.*, 1997] demonstrated fluid flow along the decollement and within the upper oceanic crust [*Silver et al.*, 2000], the latter explaining abnormally low heat flow measured in this region [*Langseth and Silver*, 1996]. *Bohrmann et al.* [2002] carried out a series of TV sled observations (OFOS) and hydrocasts to show widespread evidence of fluid seepage along the Central Costa Rica margin. *Sahling et al.* [2008] summarized evidence for more than 100 fluid seeps along the Costa Rica margin using multi-beam bathymetry, side-scan sonar, TV sled imaging, and sampling. They found an average of 1 seep site for every 4 km length of the margin. Their data showed that seeps occurred in a band centered 28 $\pm$ 7 km landward of the trench.

[8] Evidence for serpentinization beneath the Costa Rica and Nicaragua margin resulted from work by *Grevemeyer et al.* [2007] and *von Avendonk et al.* [2011] that showed seismic velocity evidence for serpentinization of subducting upper mantle beneath Costa Rica, suggesting that hydration of the oceanic lithosphere is a key mechanism for transporting fluids to the deeper parts of the mantle [*Ranero et al.*, 2003]. *Tryon et al.* [2010] found unusually high B/Li ratios in Mound 11 offshore central Costa Rica, and *Füri et al.* [2010] reported high $^3He/^4He$ ratios at Mounds 11 and 12, both indicating mantle derivation of the fluids. Several studies of BSR (representing the base of the gas hydrate layer) distribution on the Costa Rica margin have been used to constrain the thermal regime [*Ruppel and Kinoshita*, 2000; *Harris et al.*, 2010a, 2010b]. Offshore of Osa Peninsula, warmer isotherms occur at shallower levels than they do farther north off Nicoya [*Fisher et al.*, 2003; *Harris et al.*, 2010b], consistent with studies of heat flow on the incoming plate that show greater effects of fluid circulation

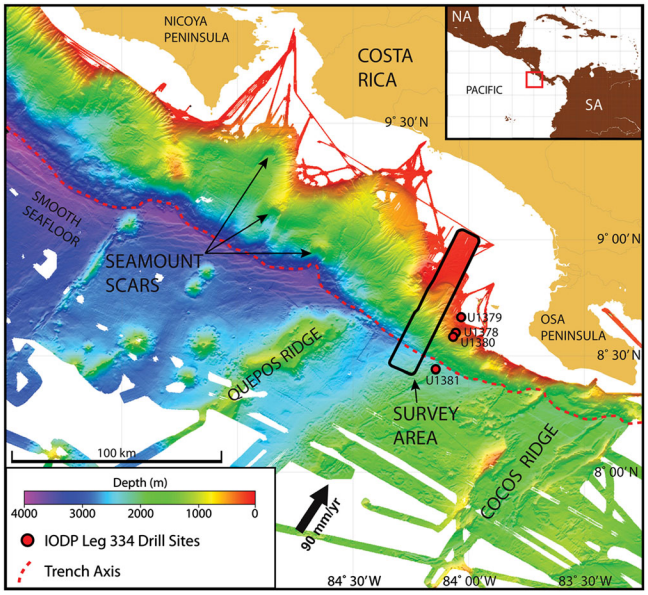

Figure 1. Color-filled multi-beam bathymetry map showing seafloor structure offshore western Costa Rica. Large 100 m grid cell bathymetry dataset collected by IFM-GEOMAR and downloaded from the Marine Geoscience Data System. Location of high-resolution CRISP survey outlined by a solid black line west of Osa Peninsula. Red box within the inset outlines the regional location of base map. White represents gaps in multi-beam coverage, whereas brown denotes land. IODP Leg 334 drill sites labeled with black-rimmed red circles. Note the lack of coverage in shallow water across the continental margin (red colors), except for the CRISP survey.

and cooling in the uppermost crust to the north [*Hutnak et al*., 2007].

[9] Studies of carbon and oxygen isotopes have documented that subduction-induced dewatering is responsible for carbonate precipitation on mounds and scarps along the Costa Rica margin [*Han et al*., 2004]. *Karaca et al*. [2010] examined sediment cores from cold seeps, finding that the rate of authigenic carbonate precipitation is enhanced at moderate fluid flow rates and is decreased at both high and low rates of flow.

[10] A relationship between increased methane emissions and seismic activity was demonstrated by *Mau et al*. [2007] in water depths of 1000 to 2300 mbsl off Costa Rica. In addition, *Brown et al*. [2005] discovered three periods of correlated seismic tremor and fluid pulsing offshore of the Nicoya Peninsula. *Ranero et al*. [2008] synthesized a large amount of fluid studies offshore Costa Rica and proposed that fluid distribution along the plate interface exerts a first-order influence on subduction erosion and on the behavior of the seismogenic zone, but that most fluid migrates to the seafloor through upper plate faulting and fracturing, rather than by flow along the décollement. Structural analyses of drill core structure across the décollement off the Nicoya Peninsula from ODP drilling legs 170 and 205 [*Vannucchi and Leoni*, 2007] indicated seismically induced fluid pulsing and changes in behavior from long-term seismic creep to short-term sudden slip

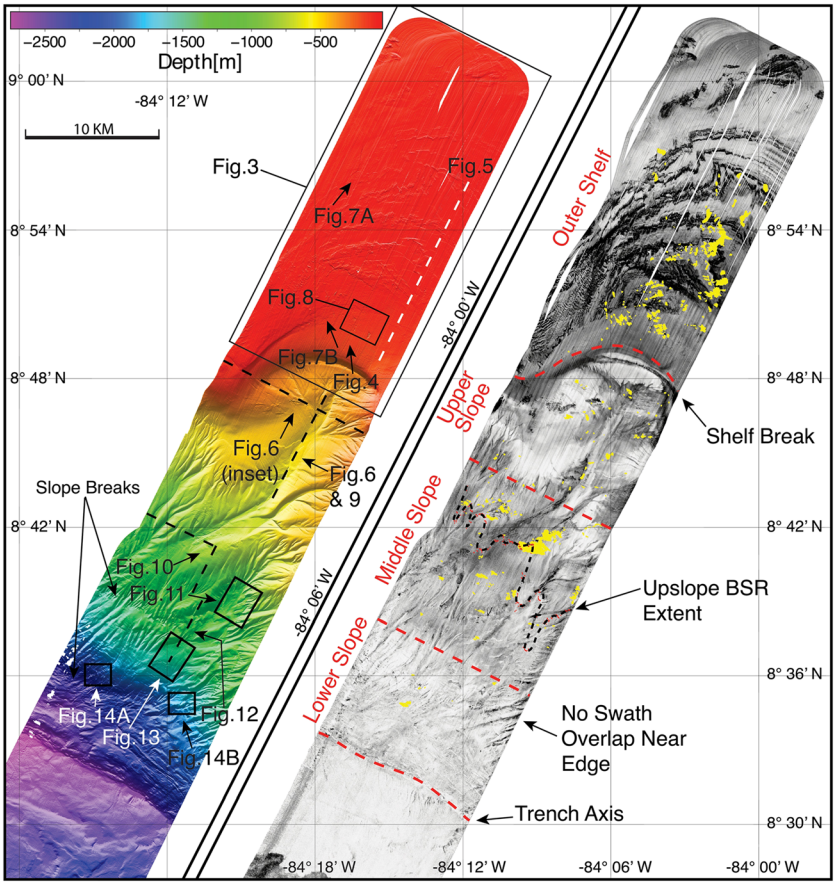

Figure 2. High-resolution multi-beam grid (10 m cell) and backscatter mosaic (5 m cell) of the 11 km wide CRISP survey area. Black boxes represent location of figures with no seismic cutaways, whereas dashed black lines represent figures with seismic lines hung from backscatter-draped bathymetry. Black and white arrows on the shaded relief bathymetry denotes viewing angle of perspective figures. Dashed white line represents location of Profile 1. Yellow patches overlaid onto the backscatter mosaic represent locations of bright spots mapped within the upper 200 m of the 3-D seismic volume. Dashed red lines separate the four margin sections, outer shelf, upper slope, middle slope, and lower slope. Dashed black line across the mid-slope of the backscatter mosaic traces the upslope termination of the BSR mapped out in the 3-D seismic volume (red dots traced with black dashed line). Dark colors indicate high-backscatter strength on backscatter plot. Note the loss in backscatter resolution and increase in canyon backscatter strength at the survey edges due to lack of overlapping swaths.

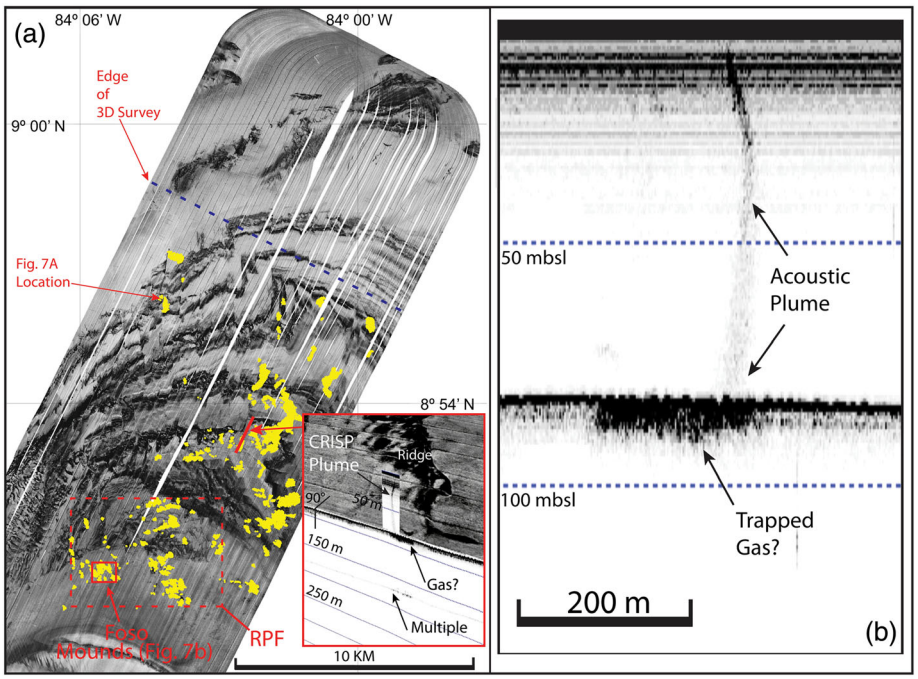

Figure 3. (a) Detailed backscatter mosaic of outer-shelf region. Overlaid yellow patches represent locations of reversed polarity bright spots mapped within the upper 200 m of the 3D seismic volume. Solid red line denotes location of 3.5 kHz profile. Dashed red box outlines location of Racimo Pockmark Field (RPF), which is shown in greater detail on Figure 9a. Solid red box shows location of Foso Mounds (Figure 3b). Dashed blue line traces the edge of the 3-D seismic survey. Inset shows perspective view (red arrow denotes look direction) of backscatter-draped bathymetry and acoustic plume imaged in the water column on a 3.5 kHz profile. (b) 3.5 kHz profile (shown in Figure 3a inset) showing acoustic plume and possible gas trapped below the seafloor.

events. These changes are associated with changing fluid pressures along the fault surface, and such changes were observed in real time [*Davis and Villinger*, 2006; *Solomon et al*., 2009; *Davis et al*., 2011] as a result of monitoring studies using a CORK observatory.

3. Geophysical Data and Methods

[11] During April and early May of 2011, we collected high-resolution multibeam bathymetry and backscatter data, in combination with an 11×55 km grid of 3-D seismic reflection data [*Bangs et al*., 2011] using 300 m line spacing, offshore and northwest of Osa Peninsula, Costa Rica (Figure 1), as part of the Costa Rica Seismogenesis Project (CRISP) 3-D seismic experiment. Multibeam data were collected across the upper shelf, slope, and trench axis using the pod-mounted Simrad EM122 $1° \times 1°$ 12 kHz deep-water sonar system onboard the R/V *MARCUS G. LANGSETH*. Because of the closely spaced tracks and use of multiple overlaps (4 to 5 times) plus 1.4 km fixed swath mode (Appendix S1 in the auxiliary material), we greatly improved the resolvability and density of the data and were able to grid shallow water bathymetry at 5 m and deep water at 10 m.[1] Backscatter data were mosaicked at 2 m and 5 m for shallow and deep water, respectively. At all depths, no features smaller than at least double the beam footprint size were interpreted and most interpreted features are at least 10 times the beam footprint size. We used an average velocity of 1700 m/s (Appendix S1) to convert time to depth on seismic profiles. Details of our methods and use of the EM122 system and the 3-D seismic system are given in Appendix S1; Figure 2 shows the resultant bathymetric grid and backscatter mosaic for the CRISP survey area.

4. Results

4.1. Structural Setting

[12] Here we explore the relationship of the structure of the southern Costa Rica Pacific margin to the geophysical indicators of fluid flow and seafloor seepage. We limit our focus to the seafloor and

[1]All Supporting Information may be found in the online version of this article.

the upper kilometer of the sub-surface structure of the margin, because deeper structure will be dealt with when the full processing of the 3-D seismic data are completed. In this paper, we utilize the high-resolvability multi-beam bathymetry and backscatter data, 3.5 kHz echo-sounder data, and the preliminary post-stack time-migrated 3-D seismic data. We will treat the margin in four sections: the outer shelf, upper slope, middle slope, and lower slope regions.

[13] The outer shelf has two distinct zones on the backscatter map. The shallower region (75 to 135 mbsl) consists of an arcuate series of high and low backscatter bands (strata), displayed because this part of the outer shelf has been eroded to expose the top of an anticline. The height or relief of the exposed high-backscatter strata ranges from <1 m up to 7 m. The outermost 3–5 km (135 to 200 mbsl) does not display this banded bedding, likely because it is buried by a sediment drape that was below the depth of wave-planed erosion during the last glacial maximum (Figure 3a). The folded layers are displaced by a dense system of faults, trending roughly N-S and E-W, and spaced an average of about 200 m apart, although spacing varies significantly from place to place. The faults show apparent horizontal displacement (Figure 4), but the sense of displacement is inconsistent (dextral and sinistral apparent offsets along adjacent faults and along a single fault trace; Figure 4 inset), making it more likely that these are normal faults, not strike-slip faults. In that case, an apparent seaward displacement

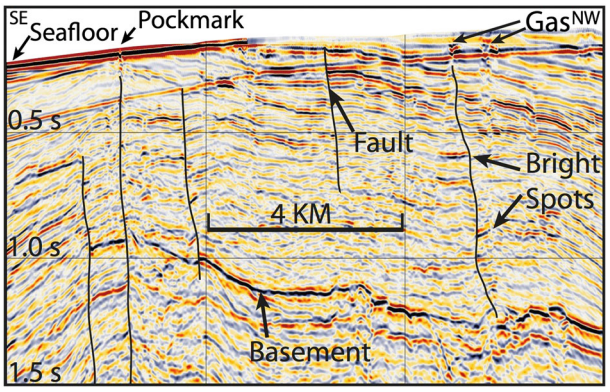

Figure 5. Seismic Profile 1 located across the outer shelf region. Seismic inline shows a large anticline above an acoustic basement high and dense faulting throughout the region. Multiple faults extend down through the acoustic basement reflection and bright spots flank faults that terminate into bright spots near the surface. Missing seafloor reflection toward the NW is due to near offset holes caused by mammal mitigation shutdowns. See Figure 2 for location.

of a landward-dipping bed is actually a downthrown block. This interpretation is consistent with observations of apparent vertical displacement on the seismic lines (Figure 5). The zone of arcuate outcropping and faulted strata overlies a large anticlinal fold that is located above a basement high (Figure 5). The shelf break, located approximately along the 250 mbsl contour is also arcuate in shape, similar to erosional scars left by subducting seamounts that are observed to the northwest (Figure 1) [*von Huene et al.*, 2000].

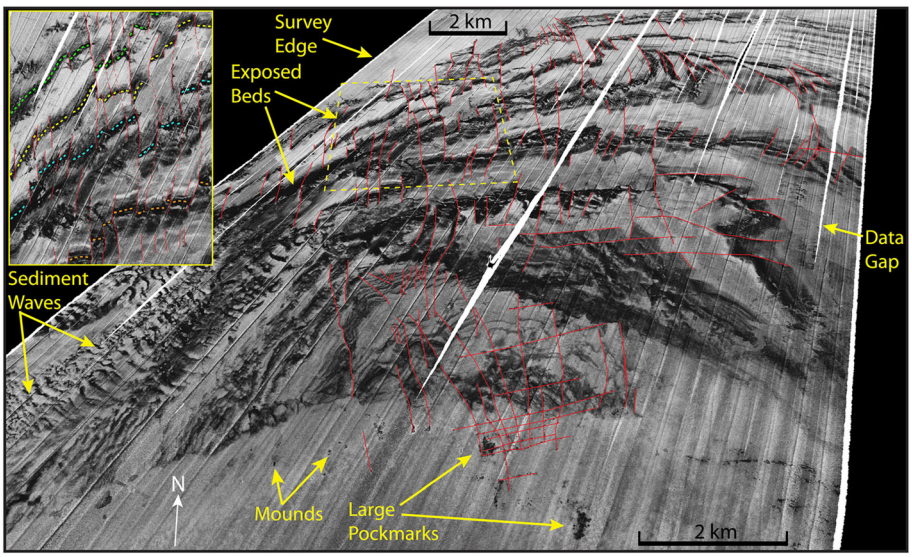

Figure 4. Perspective view of backscatter-draped bathymetry over the outer-shelf region. Solid red lines trace apparent offsets in exposed beds (high-backscatter ridges). Dashed yellow box shows location of top left inset. Inset (map view) shows offsets in exposed beds traced by colored dashed lines that have no consistent direction of offset. Note large high-backscatter pockmarks in sedimentary cover.

[14] The outermost part of the shelf does not show fault displacement because of latest Pleistocene sediment cover. However, the fault pattern mapped just to the north continues into this sedimented zone as lines of small, high-backscatter pockmarks and mounds (Figure 4), which we discuss later as evidence for fluid flow structures along the buried faults.

[15] The shallow structure of the upper (~350 to 650 mbsl) and middle (~650 to 1550 mbsl) slope regions is dominated by a series of folds trending approximately E-W extending the width of the survey, with an increase in deformation and faulting toward the east, as imaged by the multi-beam bathymetry and seismic data (Figures 2, 3, and 6). The upper and middle slope depths near the eastern edge of the survey are shallower than the western edge, and this change occurs where the Cocos Ridge has intersected the trench. The top reflection of the large fold marks a widespread unconformity that separates more intense deformation below from younger sediment infill (Figure 6). A series of canyons cut through the upper and middle slopes, some of which erode through the unconformity at the crests of folds (Figure 6). A few of the larger SW-trending canyons are linear and narrow, which may suggest fault-control (Figure 2).

[16] The structure of the lower slope (~1550 mbsl to trench axis) is composed of canyon-cut sediments, thrust faults, and two extensive breaks in slope (located at ~1350 and 2350 mbsl) that trend approximately parallel to the trench, extending across the western half of the survey (Figure 2). The breaks in slope occur above folds, whereas shorter linear breaks in the slope with a trench-parallel orientation are associated with thrust faults. The latter dominate the structure near the toe of the slope, especially along the eastern edge of the survey (Figure 2). Orientation of the trench axis and thrust faults change near the eastern side the survey, and the trench axis shoals by ~300 m from the western to eastern edge of the survey, both associated with the subduction of western edge of the Cocos Ridge (Figure 1).

4.2. Geophysical Fluid Flow Indicators

[17] Multiple geophysical indicators of potential seafloor seeps are present in bathymetry, backscatter, and 3-D seismic data and their widespread distribution ranges from the outer shelf to the lower slope region. The features we interpret to indicate surface seepage include high-backscatter pockmarks, mounds, and ridges, a large portion of which are found in clusters and in linear chains. In addition, the distribution of most seabed and

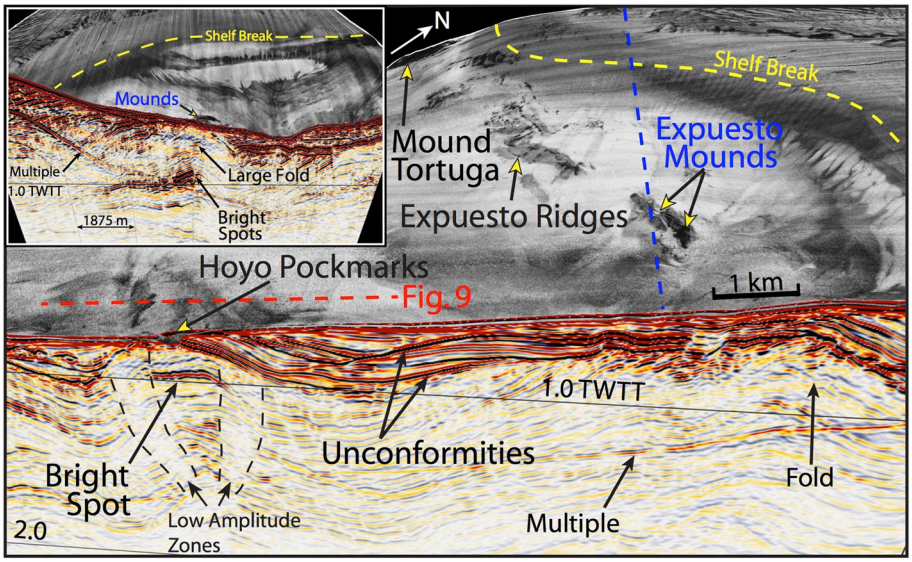

Figure 6. Perspective cutaway view of backscatter-draped bathymetry imaging the upper slope region; view is looking to the northwest. Image shows locations of Expuesto Mounds, Mound Tortuga, and Hoyo Pockmark Field. Seismic cutaway shows shallow structure below the upper slope and indicators of fluid flow below Hoyo Pockmarks. Note the unconformity that marks a clear change in reflection strength and that separates the folded sediments below from draped sediments above. Dashed blue line shows location of inset cutaway profile, and dashed red line denotes location of profiles shown in Figure 9. Dashed yellow line traces the shelf break. Inset: Perspective cutaway view of a seismic cross-line slicing through the upper slope and Expuesto Mounds (view to east). Note the large fold below the high-backscatter mounds and extensive bright spots at depth.

subsurface structure shows apparent folding and fault control. Below, we describe a select group of features representative of the potential seeps identified within the survey area. Identified surface indicators are located directly above reversed polarity bright spots and flat spots mapped within the upper 200 m of the 3-D seismic volume (Figure 3a) and near vertical zones of disturbance and reduced reflection continuity. These seismic anomalies are the same criteria commonly used to identify fluid flow and hydrocarbon leakage in the petroleum industry [*Løseth et al*., 2009]. Only high-backscatter features with additional indications of fluid seepage (e.g., mounds, pockmarks, and subsurface amplitude anomalies and flat spots) are interpreted as potential seeps. We are not able to determine whether seeps are presently active, except for an acoustic plume in the water column above a fault trace on the outer shelf.

4.2.1. Outer Shelf

[18] Located on the outer shelf near the NW corner of the 3-D seismic grid at ~85 mbsl is a series of high-backscatter strength mounds (named Osa Mounds) that have depressions or pockmarks flanking the SW sides of the mounds (Figure 7a). Mounds and associated pockmarks are clustered along a fault trace clearly imaged on the backscatter mosaic, and they lie above shallow bright spots mapped within the 3-D seismic volume (Figure 3a). The mounds are interpreted as constructional features, such as mud volcanoes, methane-derived authigenic carbonate (MDAC) mounds, or bioherms, that are younger than ~15,000 years, the time when sea level was approximately 90 m below today's level [*Siddall et al*., 2003]. The low-backscatter pockmarks next to the mounds have a slight rim of relief (up to 0.5 m) suggesting deposition from sediment ejected from the pockmark (Figure 7a).

[19] South of the exposed faulted beds near the shelf break is a cluster of high-backscatter pockmarks and mounds surrounded by relatively uniform low-backscatter intensity (Figure 8a). Some of these pockmarks attain lengths of hundreds of meters and depths of tens of meters. The pockmarks are irregular, and some contain rough internal topographies composed of local peaks and depressions, such as Pockmark Unir (Figure 8b). Three kilometers to the north is a series of linear, high-backscatter mounds directly above a large high-amplitude reversed-polarity bright spot (Figure 8c), located at the crest of an anticline approximately 30 m below the seafloor (Figure 8d). In addition, groups of high-backscatter pockmarks form linear chains that trend N-S and E-W, intersecting each other and terminating into fault traces observed in the exposed high-backscatter beds (Figures 4 and 8a). The field of pockmarks and mounds highlighted in Figure 8a suggests fluid flow concentrated near the crest of a large anticline that spans the width of the survey (Figures 8c and 8d). The approximate N-S and E-W orientations of the linear chains of pockmarks indicate fluid flow along both sets of faults (Figure 8a). Reverse polarity bright spots below the high-backscatter mounds and pockmarks are found predominantly along fault traces (Figures 3a and 8c), supporting this interpretation. Furthermore, bright spots flanking faults at depth suggest a possible deep margin-wedge source (Figure 5).

[20] High-backscatter mounds (Foso Mounds), which are a few meters high and surrounded by moat-like depressions, are also abundant near the

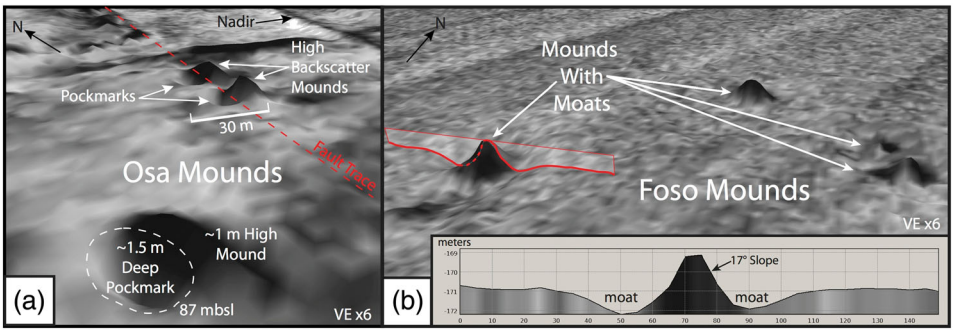

Figure 7. Seafloor seepage structures imaged on the outer-shelf region. (a) Perspective view of backscatter-draped bathymetry showing Osa Mounds with adjacent pockmarks (see Figures 3 and 4a for location). Dashed red line traces offsets in exposed bed. (b) Perspective view of Foso Mounds located near the shelf break on the outer shelf (see Figure 2 for location). Red line traces the location of inset profile view. Note the moats surrounding the high-backscatter mounds. Inset shows profile across one of the mounds showing the approximately 1 m deep moat. Color fill on profile represents backscatter strength.

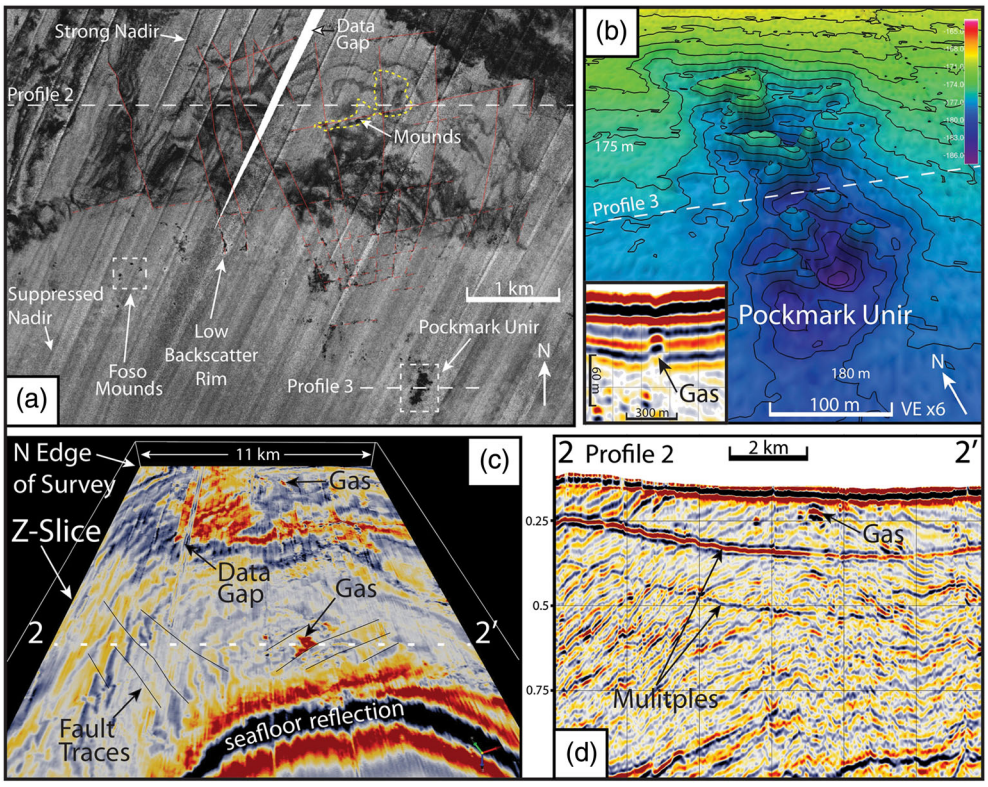

Figure 8. (a) Overhead view of backscatter mosaic showing Racimo Pockmark Field, Foso Mounds, and Pockmark Unir. Solid red lines follow fault traces apparent in exposed beds, and dashed red lines trace faults inferred by linear chains of pockmarks and mounds. Dashed yellow line shows location of large bright spot shown in Figures 8c and 8d. Note how the nadir backscatter artifact is subdued as swath overlap increases to the south with increasing depth. (b) Perspective bathymetric view of Pockmark Unir. Note complicated internal structure of highs and lows. Inset: Profile 3 across Pockmark Unir (inset) shows reverse polarity bright spot directly under the pockmark. (c) Perspective view of 3-D seismic Z-slice approximately 30 m below Racimo Pockmark Field. Dashed white line shows location of Profile 2 in Figure 8d. (d) Seismic Profile 2 located on Figures 8a and 8c. Note the reverse polarity bright spot located at the top of the anticline, just below the seafloor, sliced by the z-slice shown in Figure 8c.

shelf edge (Figure 8a). The mounds surrounded by moats imaged near the shelf break may be either seep-related carbonate mounds exposed by erosion or mud mounds, either of which may have been scoured by local currents (Figure 7b). Alternatively, the moats may have been created by fluid expulsion or collapse due to degassing of sediments below. Presence of multi-directional sand waves (Figure 4) is consistent with scouring from current erosion, whereas shallow bright spots directly below (Figure 3) may suggest subsidence due to degassing.

[21] Near the center of the outer-shelf region, an acoustic plume (CRISP Plume) was imaged in the water column using the 3.5 kHz echo-sounder, located along a fault trace (Figure 3a). CRISP plume is likely composed of gas bubbles, most likely methane, seeping from the seafloor. This inference is supported by the reversed polarity bright spot directly below (~65 mbsf) the imaged plume, strong seafloor acoustic response similar to a "gas curtain" on the 3.5 kHz profile, and the linear high-backscatter mound on the seafloor (Figure 3a inset).

4.2.2. Upper Slope

[22] Two regions of high-amplitude backscatter associated with mounds, and depressions (Figure 6) are seen on the upper slope. Both zones of high-backscatter strength overlie anticlines that have bright spots at their crests directly beneath the surface features seen on the backscatter data (Figure 6).

[23] The shallower of the two anomalies, named Expuesto Mounds, is a group of high-backscatter mounds and linear ridges that extend from the middle part of the survey to approximately 8 km to the SW (Figure 6). Below the two large (~750 by 200 m) high-backscatter mounds, seismic reflection data show that the mounds are part of an exposed unconformity at the seafloor, which extends beneath a thin veneer of sediment drape SE across the upper

slope (Figure 6). Approximately 350 m below is a series of large reversed-polarity bright spots that end abruptly to the SE against an apparent fault (Figure 6 inset). One km to the SW is a series of N-S and E-W striking high-backscatter ridges (Figure 6). Near the western edge of the survey, along the same trend line of Expuesto Mounds, is Mound Tortuga, a ~20 m high mound with very high-backscatter strength. Expuesto Mounds (Figure 6 inset) likely represent carbonate mounds, mud mounds, or older fluid flow related structures exposed by uplift and erosion. In support of the latter interpretation, older fluid flow conduits would be more resistive to erosion due to carbonate cementation and other mineral precipitation [*Judd and Hovland*, 2007] and the mounds are atop an exposed unconformity. The orientation of the linear ridges and faults imaged below can be explained by focused flow along faults (Figure 6). Additionally, high-backscatter peaks along the ridges may indicate concentrated "chimneys" of carbonate or mineral precipitation along the faults.

[24] Five kilometers SE, Hoyo Pockmark Field is a large patch of moderate to high-backscatter seafloor cut by steeply sided (up to 51°) pockmarks within two canyons trending nearly N-S and E-W (Figure 6). 3-D seismic data reveal that the canyons and local pockmarks cut into an unconformity at the top of a large anticlinal fold (Figure 6). Approximately 140 m sub-bottom is a large, abruptly ending, reversed-polarity flat spot, which is flanked by zones of reduced reflection continuity and very low amplitudes that extend from depth up to the seafloor (Figures 6 and 9). The reverse polarity bright spot below is flat, most likely indicating gas-rich or over-pressured fluids pooled below a trapping horizon. Imaged sub-vertical columnar zones of disturbed reflections with weak amplitudes bounding the large flat spot (Figure 6) are found commonly below mud diapirism, mud volcanoes, carbonate mounds, and pockmarks [*Judd and Hovland*, 2007; *Van Rensbergen et al.*, 2007], and most likely indicate zones of focused fluid flow and gas [*Løseth et al.*, 2009].

4.2.3. Middle Slope

[25] The middle slope region (~650 to 1550 mbsl) displays two linear zones of moderate to strong backscatter, a possible incipient slope failure surrounding a high-backscatter mound, and various high-backscatter strength pockmarks. The westernmost linear zone of increased backscatter strength is ~14 km long and trends NE to SW, from ~650 to

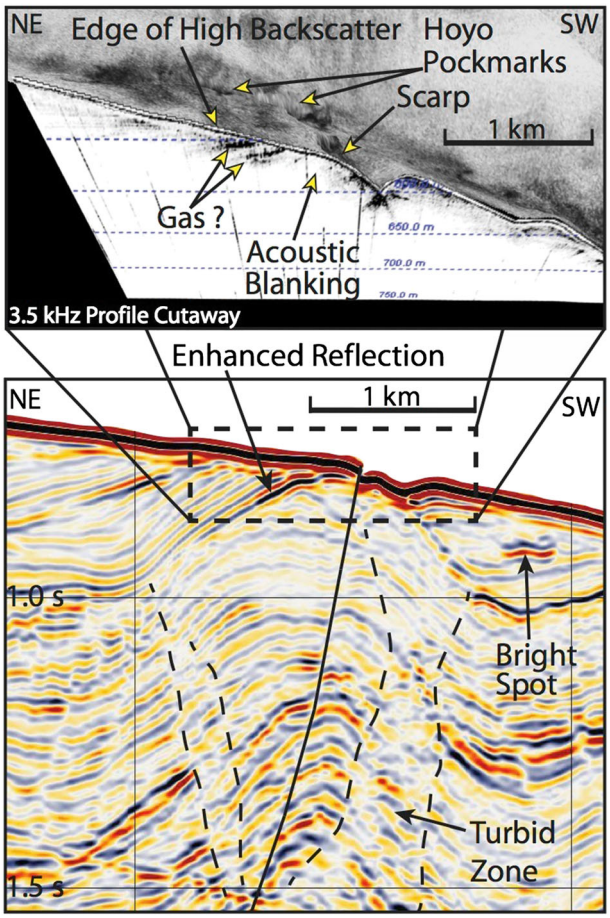

Figure 9. Bottom: Seismic reflection profile across Hoyo Pockmarks located on Figure 6. Seismic inline shows zones of low amplitudes and disturbed reflections bounding a large fold cut by a canyon at the seafloor. Solid black line traces a fault cutting through the fold, offsetting the seafloor. Dashed black box shows location of 3.5 kHz cutaway above. Top: Perspective cutaway of backscatter-draped bathymetry and a 3.5 kHz acoustic profile. Note the strong reflections interpreted to be due to gas just below the patch of high-backscatter surrounding Hoyo Pockmarks.

1525 mbsl, while to the east another, ~10 km linear zone of high backscatter follows along the upslope termination of the BSR from ~800 to 1450 mbsl (Figure 2). Adorning the ~14 km long western linear backscatter feature are Cadena Pockmarks, multiple linear closed depressions up to 20 m deep with up to 47° slopes separating two bathymetric highs (Figure 10d). Cadena Pockmarks, lying along a linear high-backscatter zone (Figure 10a), are likely young, as they show very steep sides and have not been eroded away from sediment drainage or filled in. Upslope termination of the BSR occurs under a few of the linear pockmarks (Figure 2), suggesting gas release as a possible source for pockmark

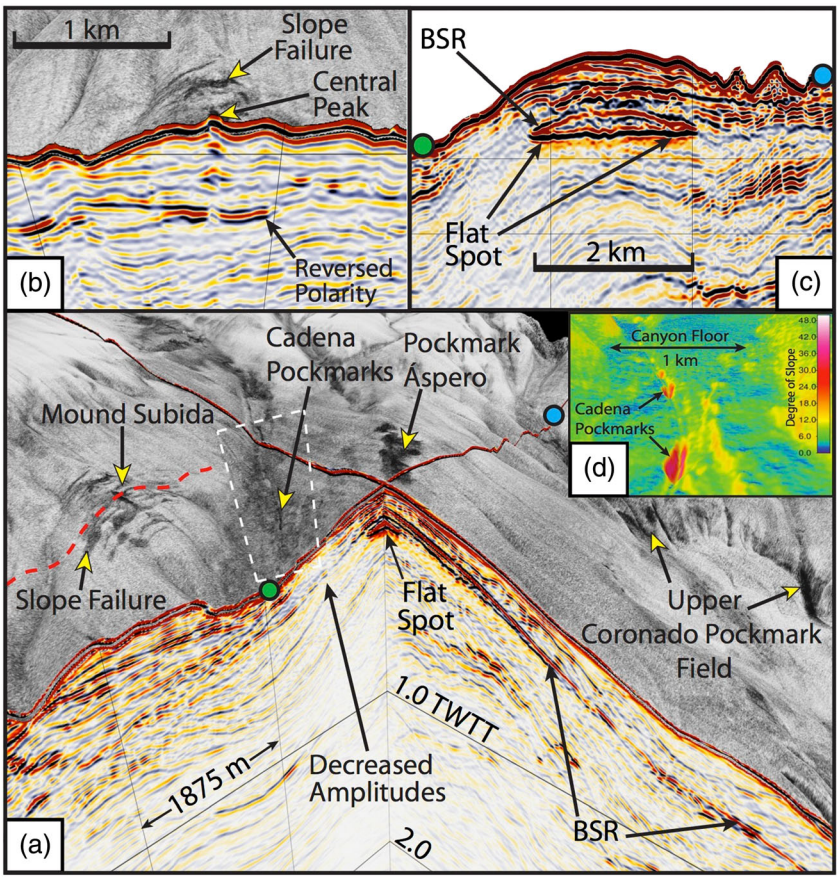

Figure 10. (a) 3-D perspective view of middle slope region looking northeast. Backscatter-draped bathymetry shows Cadena Pockmarks, Pockmark Áspero, Mound Subida, and other high-backscatter patches to the southeast located at the base of canyons. Hung seismic profiles show structure and fluid flow indicators below. Green and blue circles show location of seismic cross-line displayed in panel C. Dashed red line across Mound Subida denotes location of seismic cross-line shown in Figure 10b. Dashed white line traces a fault that cuts across the middle slope. Dashed white box shows location of Figure 10d. (b) Perspective cutaway view of Mound Subida surrounded by slope failure structures. (c) Seismic cross-line across a large fold showing the BSR and a large flat spot that both terminate at the same lateral extent. (d) Perspective view of slope gradient amplitude draped on bathymetry. Note chain of enclosed pockmarks (Cadena Pockmarks) along canyon floor.

formation, although the elongated morphology and linear distribution suggest focused flow along a fault.

[26] Atop the bathymetric high (~725 mbsl) to the NW is Mound Subida, a very high-backscatter linear ridge (~350 × 150 m and ~15 m high) surrounded by arcuate, subtle depressions of high backscatter (Figures 10a and 10b). Mound Subida lies directly over a vertical zone of reduced seismic reflection coherency and bright spots leading up from a large, shallow (~160 mbsf) reversed-polarity bright spot (Figure 10b). We interpret the series of arcuate high-backscatter depressions as incipient slope failure (Figure 10b) and Mound Subida as a mud diapir or carbonate mound. A vertical zone of disturbance imaged below Mound Subida indicates a zone of focused fluid migration and/or sediment fluidization. Upturned high-amplitude reflections below Mound Subida may indicate diapiric flow or velocity pull-up due to concentrated high seismic velocities above (e.g., carbonate cementation). Rapid degassing along this zone may have caused fluidization of sediments and destabilization, creating the plane of rupture for the incipient slope failure.

[27] Pockmark Áspero is approximately 3 km SE of Mound Subida, atop a gently sloping bathymetric high at ~690 mbsl and is composed of a large (~1500 by 300–500 m) high-backscatter patch over rugose bathymetry with low relief (Figure 10a). Below Pockmark Áspero and just below the upslope termination of the BSR is a 2 km by 350 m high-amplitude flat spot centered near the top of a large fold (Figure 10c). High-backscatter strength across

Pockmark Áspero (Figure 10a) may represent exposed carbonate or methane hydrate, chemosynthetic communities, exposed older/consolidated material, or some combination of these. The large flat spot is positive polarity and likely represents fluid trapped at the top of the fold under a lens of free gas and frozen methane hydrate above (Figure 10c). The flat spot termination is approximately that of the BSR, indicating the hydrate is likely acting as the fluid trap.

[28] Upper and Lower Coronado Pockmark Fields (Figures 11 and 12) consist of a series of high-backscatter closed depressions (pockmarks) concentrated at the basal inflection point of multiple canyons across the middle slope region. These abrupt breaks in slope can be seen throughout the mid-slope region (Figure 2), the majority of which overlie weak or absent BSR amplitudes, the upslope BSR termination, and/or back-tilted sediments on the flanks of folds (Figure 12).

[29] Cascada Pockmark within the Upper Coronado Pockmark Field is a closed depression (~10 m deep) with a possible slump scar directly upslope that appears to have removed material from a ~600 m long section of a canyon (Figure 11 inset). Cascada pockmark and surrounding smaller pockmarks straddle the abrupt upslope termination of the hydrate BSR (Figure 11). The abrupt termination observed below Cascada Pockmark and across the middle slope could suggest recent hydrate instability and methane release, similar to that observed by *Bangs et al*. [2010] across the Nankai Trough offshore southwestern Japan. To the west along the mid-slope region, 3-D seismic reflection data reveal a fold under Lower Coronado Pockmark Field that extends across the middle slope (Figure 12). The pockmarks are closed depressions, most of which are a few to tens of meters deep (Figures 12b and 12c). BSR amplitudes are very weak or absent across the highly tilted sediments on the sides of the fold but are present with higher amplitudes atop the folds (Figure 12). Figure 12 shows a sub-bottom reflection below a slope-break pockmark that continues down along the same slope as the canyon. This reflection appears to represent the paleo-floor of the canyon. Note the reverse polarity bright spot along the tilted and deformed beds below the buried canyon floor, likely indicating gas-rich fluid concentrations [*McConnell and Kendall*, 2003]. Most canyons with pockmarks within Upper and Lower Coronado Pockmark Fields show high-backscatter strength, even after averaging 4-to-5 overlapping swaths, suggesting that these select canyons expose older consolidated material or that they act as zones of focused fluid seepage upslope [*Jobe et al*., 2011]. The presence of pockmarks at the base of the canyons and reverse polarity bright spots below the buried canyon floors support the latter interpretation. In addition, chains of small pockmarks, such as Rabo Pockmark Field (Figure 13), are present across the middle slope, commonly above weak or absent BSR amplitudes. Similar to the outer shelf region, the linear

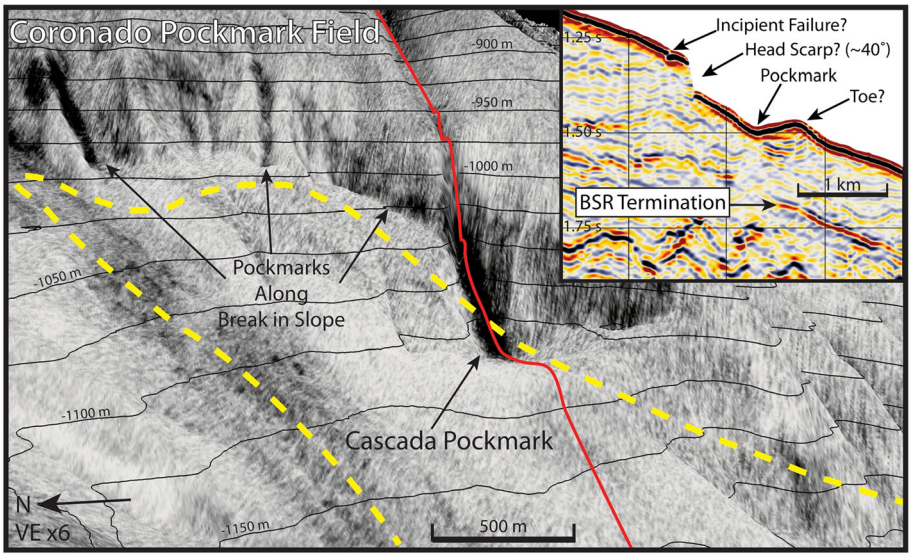

Figure 11. Perspective view of backscatter-draped bathymetry looking east showing the upper portion of Coronado Pockmark Field and Cascada Pockmark. Dashed yellow line traces the approximate location of the upslope BSR termination. Red line shows location of seismic line shown in the inset. Inset: Seismic line extracted from 3-D volume along the axis of Cascada Pockmark and along the canyon upslope. Note the possible incipient failure and very steep (~ 40°) slope directly above the pockmark and termination of the BSR below.

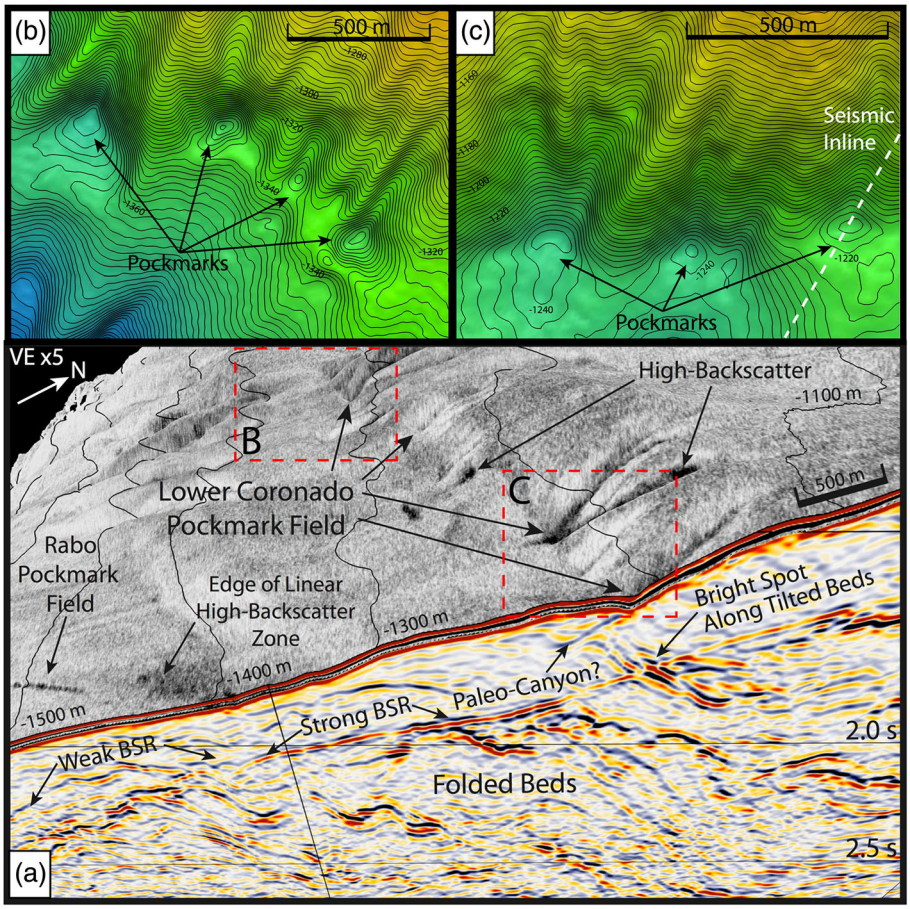

Figure 12. (a) Perspective view of seismic inline hung from backscatter-draped bathymetry located along the middle slope region (see Figure 2 for location). Backscatter draped on bathymetry shows lower Coronado Pockmark Field located along a break in slope above folded beds imaged on the seismic profile. Note the changes in the BSR strength across folded sediments and the negative polarity bright spot along a tilted reflection located below the pockmarks. Dashed red boxes show approximate locations of Figure 12b and 12c. (b and c) Map views of shaded bathymetry showing pockmarks at the base of canyons. Dashed white line on Figure 12c shows location of seismic line in Figure 12a.

orientation of the pockmark chains likely indicates focused fluid flow along fault traces.

4.2.4. Lower Slope

[30] The lower slope region (~1550 mbsl to trench axis) is characterized by generally low backscatter strength (Figure 2) with moderate to high-backscatter pockmarks commonly found along fault traces. Figure 14a shows a chain of small (120 m across and 15 m deep), high-backscatter pockmarks trending N-NW that extend from ~2080 to 2180 mbsl and fall along an arcuate break in slope interpreted as a fault trace. In addition, Mound Cima (Figure 14b) is a 100 m high mound located toward the eastern side of the survey at ~1800 mbsl, in an area that also shows high to moderate backscatter pockmark-like structures, similar to those described in Upper and Lower Coronado Pockmark Fields. The majority of the high-backscatter pockmarks cluster along trench parallel fault traces (Figure 14a). This pattern suggests focused fluid flow along thrust faults on the lower slope. Mound Cima (Figure 14b) is interpreted as mud diapirism and/or a carbonate mound. Moderate backscatter strength across the mound suggests sediment burial and limited amounts of carbonate or chemosynthetic communities at or near the surface.

5. Discussion

5.1. Numerous Seafloor Seepage Indicators and Distribution

[31] Previous studies [*von Huene et al.*, 2000; *Vannucchi et al.*, 2003; *Ranero et al.*, 2008, *Sahling*

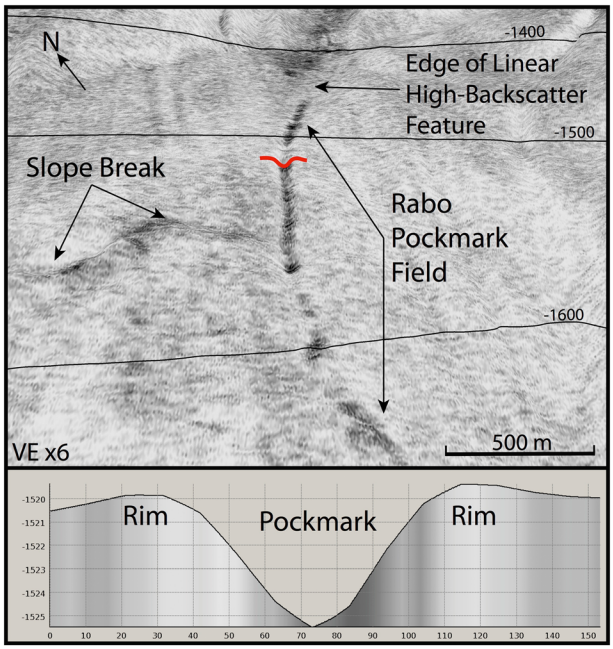

Figure 13. (Top) Perspective view of Rabo Pockmark Field located at the base of the middle slope. Backscatter-draped bathymetry shows a chain of moderate-to-high-backscatter pockmarks located at the edge of the easternmost linear zone of high backscatter. Red line denotes location of profile shown below. (Bottom) Profile of a pockmark located near the middle of the pockmark chain. Note the low-backscatter rims. Shading below seafloor indicates backscatter strength.

et al., 2008, *Mau et al*., 2012] showed that the western Costa Rican margin is erosive with a highly fractured slope margin, allowing a higher degree of fluids and gases to permeate through the margin slope instead of flowing predominantly along the décollement toward the trench and frontal prism. The synthesis by *Ranero et al*. [2008] included 124 fluid seeps discovered across the ~500 km wide margin, most of which are reported by *Sahling et al*. [2008], and the authors suggested this number may be increased by a factor of 2 or 3 due to unmapped faults and fractures and/or resolution limitations. *Sahling et al*. [2008] reported no fluid seepage features within the 11 km wide CRISP survey area using 100 m grid cell bathymetry and 6 m pixel towed side-scan data. However, within the 11 km wide portion of the margin mapped during the CRISP survey (Figure 1), we have identified indicators of 161 possible fluid seeps across the margin. These include high-backscatter pockmarks, mounds, and ridges, the majority of which have bright spots, flat spots, or vertical zones of disturbance directly below, imaged in 3-D seismic data. The identified features range from a few meters to hundreds of meters across, and their distribution varies from isolated features to clusters and linear chains. At least 77 potential seeps are present on the outer-shelf region, 19 within the upper slope, 49 on the middle slope, and 16 across the lower slope. Pockmarks and mounds that are clearly merged were counted as one feature.

[32] Although not yet sampled geochemically or photographed and confirmed as seep sites, this 11 km wide portion of the margin (in which no potential seeps were previously reported) potentially contains a significantly larger density of seeps than reported by *Sahling et al*. [2008] and synthesized by *Ranero et al*. [2008]. In addition, no geophysical indicators of potential seeps were reported within

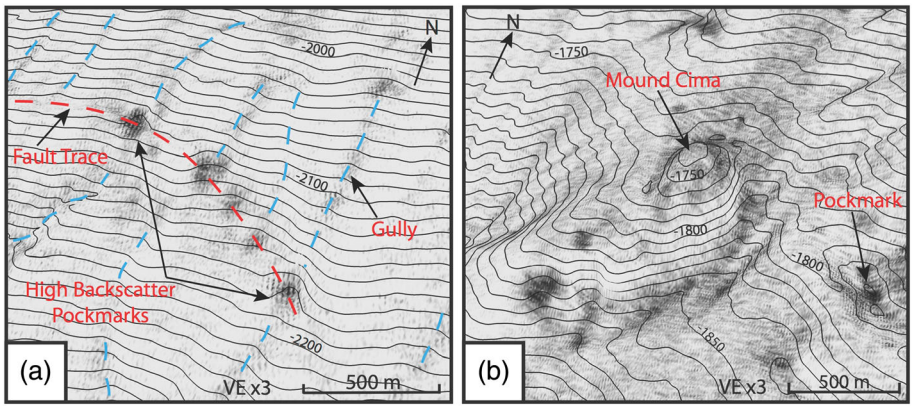

Figure 14. Perspective views of backscatter-draped bathymetry on the lower slope (see Figure 2 for locations). (a) Chain of high-backscatter pockmarks traced with dashed red line. Pockmarks are located along a break in slope interpreted as a fault trace. Canyons are traced with dashed blue lines. (b) Moderate backscatter strength mound located near the eastern edge of the survey. Note surrounding patches of high-backscatter and nearby high-backscatter pockmark.

the CRISP survey area. The high density of geophysical seep indicators suggests either (i) this zone is more heavily fractured and deformed by the projection of the Quepos Ridge or subducting Cocos ridge than other parts of the Costa Rica margin, resulting in increased permeability and fluid flow through the margin, or (ii) the very high-resolvability of the CRISP multi-beam and backscatter data reveal features that were not easily identifiable with previously collected datasets (Figure 3A in Appendix S1). Within the CRISP survey, we imaged features on the outer-shelf as small as 15–30 m across with 0.5 m relief, well above the 2.6 m beam footprint size at 150 mbsl. At all depths within the survey region, no features smaller than twice beam footprint were interpreted. The fact that no seep indicators were mapped previously across the CRISP swath using conventional hull-mounted multi-beam and towed side-scan data [*Sahling et al*., 2008] could indicate (in contrast with (i)) that there are a significant proportion of smaller seepage features across the previously mapped 500 km long margin, suggesting a substantially greater density of seeps than previously reported.

[33] Although shallow seeps have been documented globally [*Judd and Hovland*, 2007], they have not been reported offshore Costa Rica or Panama. *Sahling et al*. [2008] concluded that the majority of seafloor seeps across the southern Nicaragua and northern Costa Rican margins were concentrated along a band at mid-slope depths, with a few seeps located along the lower and upper slopes and no seeps shallower than the shelf break. Similar to these findings, our results show a large proportion of fluid seep indicators across the mid-slope region, with fewer interpreted seep features along the lower and upper slopes. However, in contrast to *Sahling et al*. [2008], who had very limited shallow water multi-beam coverage and found no seeps shallower than the upper slope, approximately half of the 161 potential seep sites interpreted in this study were discovered along the 11 km wide portion of the outer shelf southwest of Osa Peninsula.

[34] The abundance of potential fluid seepage sites across the outer shelf may be due in part to deformation and faulting caused by the subduction of the projected Quepos Ridge. The arcuate shape of the shelf break (Figures 2 and 6) supports an interpretation of seamount/ridge subduction. Such high seep concentrations on the outer shelf observed in this study suggests that shallow seeps may be abundant across the whole margin, especially in regions of recent seamount subduction.

5.2. Pockmarks Located Along Slope Breaks at the Foot of Canyons

[35] Pockmarks, and their relationship to erosional canyons, have been recently documented and studied on the West African margin [*Gay et al*., 2003, 2006; *Pilcher and Argent*, 2007; *Jobe et al*., 2011], on the Brazilian margin [*Heinio and Davies*, 2009], and on the West Baja California margin [*Kluesner and Lonsdale*, 2010]. Offshore of the West African margin, two models for pockmark formation in canyons or in linear chains have been proposed: (i) pockmark chains are precursors to canyon or gully formation [*Pilcher and Argent*, 2007] and (ii) pockmark chains form after canyon abandonment [*Jobe et al*., 2011]. Using 3-D seismic reflection data, *Jobe et al*. [2011] showed that the chains of pockmarks and canyons with ridges offshore West Africa formed due to canyon abandonment, where sediment supplies to the canyons were very low and the erosional heads were cut off, allowing sediment to infill the canyon, except where fluids are exiting the seafloor. This scenario is very similar to the Western Baja margin where very large pockmarks in trains and within canyons have formed along a part of the margin that has been cut off from the terrigenous supply due to the development of a trans-tensional basin. Furthermore, *Sun et al*. [2011] studied chains of pockmarks as well as isolated mega-pockmarks (>3 km diameter and >160 m deep) in the South China Sea and found evidence of fluid migration along depositional boundaries and paleo-canyon floors, suggesting these horizons provide pathways of least resistance to the seafloor.

[36] Upper and Lower Coronado Pockmark Fields, located along the mid-slope region in the CRISP survey, are composed of pockmarks clustered at the foot of multiple canyons (Figures 11 and 12). Although the canyons terminate into the pockmarks (Figures 12b and 12c), multiple extensions of canyon floors have been imaged with 3D seismic data and can be seen to extend downslope past the break in slope imaged with bathymetry (Figure 12a). Multi-beam and seismic data indicate that folding and deformation of the margin sediments caused uplift and leveling of canyon slopes atop a large fold that cuts across the mid-slope (Figure 12a). The fold appears to have uplifted the sediments and flattened the slope gradients of the canyons, generating tilted beds on the flanks of the folds. Unlike canyon abandonment observed off West Africa [*Jobe et al*., 2011] and Baja California [*Kluesner and Lonsdale*, 2010], these canyons were likely abandoned due to uplift, which would inhibit

further erosion and facilitate infill of the paleo-canyon floor.

[37] Figure 12a shows back-tilted beds directly below a high-backscatter pockmark within the Lower Coronado Pockmark Field located along the base of the small canyons. These pockmarks fall along a break in the slope gradient (Figure 2). Reversed polarity bright spots along the back-tilted beds below the pockmarks and canyons suggest concentrated gas and up-dip focused fluid flow along the folded beds. Furthermore, the surrounding weakened BSR amplitudes may suggest hydrate instability above the highly tilted beds. Below the pockmarks are buried paleo-canyon reflections that link-up with canyons imaged on the seafloor (Figure 12). This relationship may suggest a possible scenario in which (i) deformation causes folding and uplift of slope sediments, (ii) concentrated fluid flow along the tilted beds intersects the paleo-canyon floors, (iii) porous canyon floors provide a least-resistance migration pathway for fluid and/or gas towards the seafloor, and (iv) fluid and gas escaping the seafloor at the canyon base result in pockmark formation.

[38] Alternatively, high-backscatter strength observed within the canyon floors could reflect over-consolidated sediments exposed by canyon erosion, however only a select number of canyons show high-backscatter, which are also located above pockmarks (Figures 11 and 12). Although we are not able to rule out other processes such as canyon erosion processes with our surface data, sub-surface data suggest it is likely that Upper and Lower Coronado Fields indicate fluid/gas expulsion along the canyon floors. As mentioned above, the majority of pockmarks imaged within Upper and Lower Coronado Pockmark Fields are located above tilted beds with reverse polarity bright spots and/or BSR amplitude weaknesses and terminations. This connection with common sub-surface indicators of fluid flow and gas concentrations [*Løseth et al.*, 2009] supports a pockmark formation mechanism related to gas and/or fluid expulsion.

5.3. Structural Controls on Fluid Flow

[39] Evidence of fluid flow along faults offshore Costa Rica has been previously identified with submersible dives [*Kahn et al.*, 1996; *McAdoo et al.*, 1996; *McIntosh and Silver*, 1996], side-scan sonar, and photography [*Sahling et al.*, 2008], although *Sahling et al.* [2008] found that fault seepage was difficult to detect and confined predominantly to the mid-slope region. *Sahling et al.* [2008] concluded that ready detection of fault seepage was not possible based on the available geophysical data and only three fault segments were included in the total seep inventory.

[40] In contrast with earlier studies, throughout the 11 km CRISP swath extending from the outer shelf to the trench, we find that numerous pockmarks and mounds form linear chains along fault traces. Offsets in exposed beds on the outer shelf allow clear mapping of fault traces (Figure 4), and numerous interpreted fluid seepage structures are clustered along the faults (Figures 4–10). In addition, shallow bright spots mapped within the 3D seismic volume below the outer shelf adorn multiple fault traces that are associated with potential seepage structures imaged on the seafloor (Figures 3, 5, and 8a). These results differ from earlier seep studies on the margin [*Sahling et al.*, 2008; *Ranero et al.*, 2008] in that we have identified widespread potential seepage structures on the outer shelf, whose distribution is controlled largely by dense faulting imaged with both bathymetry and 3-D seismic data (Figures 4 and 5). Although not as evident as on the outer shelf, seepage features on the margin slope are also partly controlled by faulting (Figures 6, 9, and 10). As was suggested by *Sahling et al.* [2008], seeps located along faults appear to be focused at discrete points, such as the high-backscatter peaks that we observe on Expuesto Ridges on the upper slope (Figure 6) and pockmark and mound chains within Racimo Pockmark Field (Figure 8a).

[41] Results from the CRISP survey suggest that dense faulting on the Costa Rican margin provides abundant conduits for focused fluid flow through not only the over-riding plate slope region but also through the shallower outer shelf region (Figure 15). Also, bright spots flanking faults at depth (Figure 5) may imply deeply sourced fluids, with faults providing permeable pathways up through the thick sedimentary section. Furthermore, multiple faults mapped across the outer shelf cut the entire sedimentary section through to the acoustic basement reflection (Figure 5), possibly tapping into a deeper margin wedge source (Figure 15). Subduction of a seamount or ridge, such as the projection of the Quepos Ridge (Figure 1), may be responsible for the dense faulting and fluid seepage observed on the outer-shelf. Additionally, the large number of seep-related structures identified on the outer shelf in the CRISP high-density multi-beam survey, and the lack of shallow seeps identified in previous surveys, may be due to the coverage and high resolvability of our datasets.

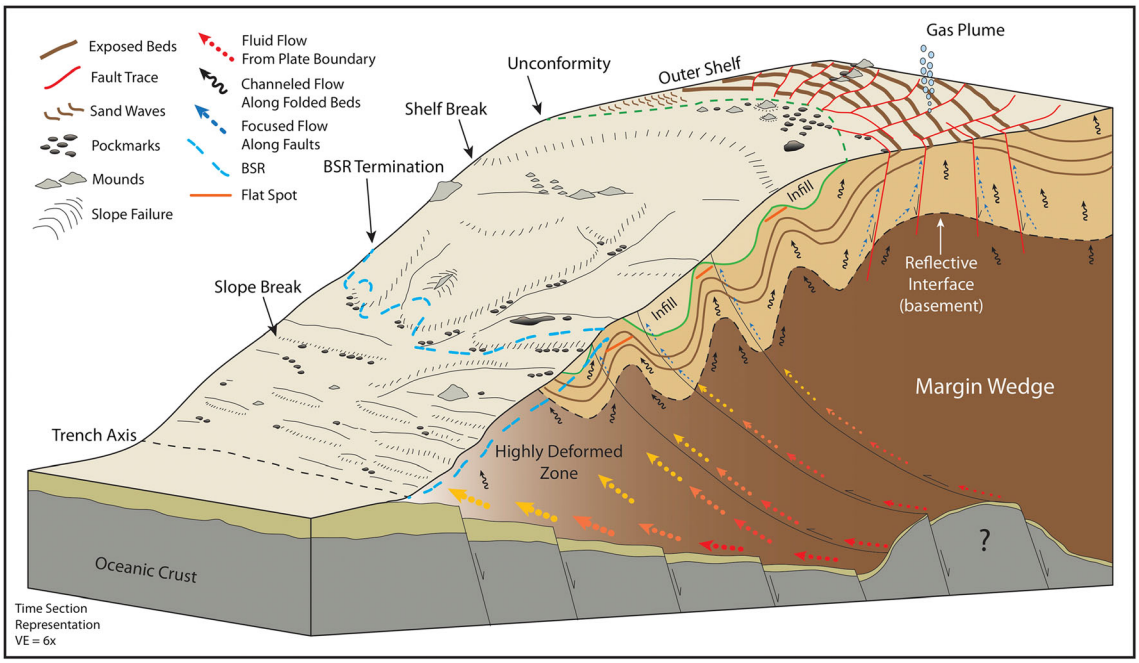

Figure 15. Conceptual 3-D block diagram of fluid flow paths and seafloor seepage features within the CRISP survey area. Locations of seafloor seepage features are strongly dependent on folds and fault patterns. Exposed beds on the outer shelf highlight dense faulting through a large anticline. Migrating fluids and gases use faults and folded stratigraphic horizons as conduits to the seafloor. Note increase in deformation to the east caused by the incoming Cocos Ridge.

[42] In addition to fault control on fluid flow and seafloor seepage, sub-surface data indicate that widespread folds channel fluids and gases toward the anticlinal crests. Below the outer shelf region, 3-D seismic data reveal a large anticlinal fold that is planed away at the seafloor (Figure 8d) and cut by numerous faults located above a basement high (Figure 5). The crest of this fold is located under Racimo Pockmark Field (Figure 8a), and reverse polarity bright spots are clustered atop the fold (Figure 3). This pattern continues downslope, with bright spots (Figure 6) and flat spots (Figure 10c) located at the tops of folds trending across the survey. Furthermore, reverse polarity bright spots (Figure 12) and sub-vertical zones of disturbance and reflection discontinuities (Figure 9) are found along the highly tilted beds on the sides of folds, likely indicating concentrated gas and fluid flow.

5.4. Implications for Seafloor Seepage

[43] Anomalous amplitude features (e.g., bright spots, flat spots, BSR, and phase reversals) and anomalous patterns (e.g., sub-vertical zones of disturbance and reflection discontinuities) imaged below potential seeps in this study have long been used as identifiers of the presence, migration, and leakage of gas and fluids [*Løseth et al.*, 2009]. Multiple examples of subsurface fluid flow and leakage indicators are present throughout the CRISP 3D seismic volume, the majority of which lead up to or are directly below high-backscatter indicators of potential seeps imaged on the seafloor (Figures 6 and 8–12). These indicators include pockmarks, mounds, and ridges that show moderate-to-high-backscatter strength, implying an increase in seafloor impedance, seafloor roughness, and/or volumetric scatter. It has been shown that methane-derived carbonates and chemosynthetic communities can lead to all three effects [*Orange et al.*, 2010] and this interpretation is consistent with multiple geoacoustic seafloor studies conducted across the Costa Rican margin (Figure 3A in Appendix S1) [*Klaucke et al.*, 2008; *Sahling et al.*, 2008; *Peterson et al.*, 2009]. Additionally, on the outer shelf, a ~90 m tall acoustic plume was imaged directly above a high-backscatter ridge underlain by a large bright spot, suggesting active venting of gas bubbles (Figure 3 inset). Potential seep features with very high-backscatter strength may be active (as we have no data to suggest they are not); however, a large proportion of identified seeps are likely episodic and currently dormant. Some potential seep features with moderate-to-low backscatter strength are likely partially buried by sediment (1–2 cm to 1–2 m) [*Klaucke et al.*, 2008], such as Mound Cima (Figure 14b). Evidence of gas pockets under a large proportion of the seeps, such as reverse polarity bright spots, suggests seeps may

become active when trapped gas pockets become over-pressured, resulting in trap leakage and subsequent seafloor seepage.

[44] While seafloor seepage sites have been well documented and measured across the Costa Rican margin slope, individual estimates of the methane seepage are spatially limited and rely on the extrapolation of seepage features identified by geophysical tools to estimate and model contributions to the global methane budget [*Klaucke et al.*, 2008]. Although not confirmed as seeps with photography and sampling, geophysical results from this study suggests seep density is likely much higher per linear km across the Costa Rican margin than previously thought [*Sahling et al.*, 2008]. Furthermore, results from this study suggest a much wider distribution of potential seeps than previously mapped, with a high density of potential seeps associated with faulting on the outer shelf region. Thus, deformation and fluid flow occur on the margin tens of km more landward than previously suggested [*Ranero et al.*, 2008].

6. Conclusions

1. High-resolution bathymetry and backscatter data (2–10 m grid/mosaic cell) have been used to indentify indicators of potential seafloor seepage sites across the 11 km wide swath of the CRISP survey located offshore southern Costa Rica. High-backscatter bathymetric features such as mounds, ridges, and pockmarks have been used as criteria to identify potential seafloor seepage structures. Directly below the majority of identified potential seafloor seeps are high-amplitude, commonly reversed polarity, abruptly ending amplitude anomalies and zones of seismic disturbance, which have been mapped throughout the upper 200 m of the entire 3-D seismic volume. We interpret these anomalies to indicate fluid migration and concentrated gas below potential seafloor seeps. Using these criteria, we have identified 161 potential seafloor seepage features, including an acoustic water column plume, throughout the 11 km CRISP swath, extending from the outer shelf to the trench axis.

2. Our results show that faulting largely controls the distribution of fluid seeps identified within the CRISP survey. Chains of pockmarks and mounds imaged on the outer shelf occur along fault traces offsetting the exposed beds and also along extensions of faults buried by sediment near the shelf break. The faults on the outer shelf appear to be normal faults, because apparent horizontal displacement directions are not consistent and faults show normal displacement in seismic lines. Seeps along faults can also be seen on the margin slope as well, such as linear chains of pockmarks and linear mounds and ridges.

In addition to intense faulting, folds appear to funnel fluids upward toward their anticlinal crests (Figure 15). Gas and fluid become trapped near the crests of folds, imaged as bright spots and flat spots in the 3-D seismic volume. Potential seafloor seepage features on the outer shelf and slope regions are commonly located along the crests of anticlines imaged within the 3-D seismic volume. In addition, pockmark fields throughout the mid-slope region are located at the termination of multiple small canyons. Folding across canyons likely resulted in canyon abandonment and concentrations of pockmarks along the break in slope.

3. The arcuate shape of the shelf edge imaged in this study and the projection of the Quepos Ridge suggests that the CRISP area is a zone of former zone seamount/ridge subduction, a process that can create structural and stratigraphic fluid/gas pathways upwards through the continental margin. The high density of potential seeps identified in this study is consistent with regions of seamount subduction, which have recently been shown to be areas of high methane flux on the Costa Rican margin [Mau et al., 2012].

4. Compared to conventional multi-beam bathymetry collected in the same region, the high-geologic resolvability of the overlapping CRISP multi-beam and backscatter datasets increases the continuity of seafloor structures, because the threshold for detection is much lower. Therefore, we image a larger proportion of potential seep features than lower resolution, more commonly acquired surveys. As no seeps were previously reported across the CRISP survey, it is possible that data of similar geologic resolvability collected elsewhere across the margin would reveal similar densities and distribution of potential seeps. Although not yet visually confirmed as seeps, geophysical results from this study suggests a more widespread seep distribution and a higher density of seeps across the Costa Rican margin than reported previously.

Acknowledgments

[45] We thank the captain, crew, and scientific party of the R/V *MARCUS G. LANGSETH* for their untiring efforts in

collecting this dataset. We also thank two anonymous reviewers and the editor for their helpful and constructive reviews. This work has been supported by NSF grants OCE-0851529 and OCE-0851380.

References

Avendonk, H. J. A., W. S Holbrook, D. Lizarralde, and P. Denyer (2011), Structure and serpentinization of the subducting Cocos plate offshore Nicaragua and Costa Rica, *Geochem. Geophys. Geosyst.*, *12*, Q06009, doi:10.1029/2011GC003592.

Bangs, N. L., M. J. Hornbach, G. F. Moore, and J.-O. Park (2010), Massive methane release triggered by seafloor erosion offshore southwestern Japan, *Geology*, *38*, 1019–1022, doi:10.1130/G31491.1.

Bangs, N. L., et al. (2011), Preliminary results of the CRISP 3D seismic experiment, offshore Costa Rica (abs), *Amer. Geophys. Un. Fall Meeting*, San Francisco, CA

Bilek, S. L., S. Y. Schwartz, and H. R. DeShon (2003), Control of seafloor roughness on earthquake rupture behavior, *Geology*, *31*, 455-458, doi:10.1130/0091-7613(2003).

Bohrmann, G., et al. (2002), Widespread fluid expulsion along the seafloor of Costa Rica convergent margin, *Terra Nova*, *14*(2), 69–79, doi:10.1046/j.1365-3121.2002.00400.

Brown, K. M., M. Tryon, H. R. DeShon, L. M. Dorman, and S. Y. Schwartz (2005), Correlated transient fluid pulsing and seismic tremor in the Costa Rica subduction zone, *Earth and Planet. Sci. Lett.*, *238*, 189-203, doi:10.1016/j.epsl.2005.06.055.

Christeson, G. L., K. D. McIntosh, and T. H. Shipley (2000), Seismic attenuation in the Costa Rica margin wedge: Amplitude modeling of ocean bottom hydrophone data, *Earth Planet. Sci. Lett.*, *179*, 391-405.

Davis, E. E., and H. W. Villinger (2006), Transient formation fluid pressures and temperatures in the Costa Rica forearc prism and subducting oceanic basement: CORK monitoring at ODP Sites 1253 and 1255, *Earth Planet. Sci. Lett. 245*(1–2), 232–44, doi:10.1016/j.epsl.2006.02.042.

Davis, E., M. Heesemann, and K. Wang (2011), Evidence for episodic aseismic slip across the subduction seismogenic zone off Costa Rica: CORK borehole pressure observations at the subduction prism toe, *Earth and Planet. Sci. Lett.*, *306*, 299-305, doi:10.1016/j.epsl.2011.04.017.

DeShon, H. R., S. Y. Schwartz, S. L. Bilek, L. M. Dorman, V. Gonzalez, J. M. Protti, E. R. Flueh, and T. H. Dixon (2003), Seismogenic zone structure of the southern Middle America Trench, Costa Rica, *J. Geophys. Res.*, *108*, doi:10.1029/2002JB002294.

Field, M. E., and A. E. Jennings (1987), Seafloor gas seeps triggered by a northern California earthquake, *Mar. Geol.*, *77*, 39-51.

Fisher, A. T., C. A. Stein, R. N. Harris, K. Wang, E. A. Silver, M. Pfender, M. Hutnak, A. Cherkaoui, R. Bodzin, and H. Villinger (2003), Abrupt thermal transition reveals hydrothermal boundary and role of seamounts within the Cocos Plate, *Geophys. Res. Lett.*, *30* (11), 1550, doi:10.1029/2002GL016766.

Fisher, D. M., T. W. Gardner, J. S. Marshall, P. B. Sak, and M. Protti (1998), Effect of subducting sea-floor roughness on forearc kinematics, Pacific coast, Costa Rica, *Geology*, *26*, 467–470, doi: 10.1130/0091-7613

Füri, E., D. R. Hilton, M. D. Tryon, K. M. Brown, G. M. McMurtry, W. Brückmann, and C. G. Wheat (2010), Carbon release from submarine seeps at the Costa Rica fore arc: Implications for the volatile cycle at the Central America convergent margin, *Geochem. Geophys. Geosyst.*, doi:10.1029/2009GC002810.

Gardner, T. W., D. Verdonck, N. Pinter, R. Slingerland, K. Furlong, T. F. Bullard, and S. G. Wells (1992), Quaternary uplift astride the aseismic Cocos Ridge, coast of Costa Rica, *Geol Soc. Am. Bull.*, *104*, 219–232.

Gay, A., M. Lopez, P. Cochonat, N. Sultan, E. Cauquil, and F. Brigaud (2003), Sinuous pockmark belt as indicator of a shallow buried turbiditic channel on the lower slope of the Congo Basin, West African Margin. In: Van Rensbergen, P., R. R. Hillis, A. J. Maltman, and C. K. Morley (Eds.), Subsurface Sediment Mobilization, *Geological Society of London, Special Publications*, *216*, 173-189, doi:10.1144/GSL.SP.2003.216.01.12.

Gay, A., M. Lopez, P. Cochonat, M. Séranne, D. Levaché, and G. Sermondadaz (2006), Isolated seafloor pockmarks linked to BSRs, fluid chimneys, polygonal faults and stacked Oligocene-Miocene turbiditic palaeochannels in the Lower Congo Basin, *Mar. Geol.*, *226*, 25-40, doi:10.1016/j.margeo.2005.09.018.

Géli, L., P. Henry, T. Zitter, et al., (2008), Gas emissions and active tectonics within the submerged section of the North Anatolian Fault zone in the Sea of Marmara, *Earth Planet. Sci Lett.*, *274*, 34-39, doi:10.1016/j.epsl.2008.06.047.

Grevemeyer, I., et al. (2004), Fluid flow through active mud dome Mound Culebra offshore Nicoya Peninsula, Costa Rica: Evidence from heat flow surveying, *Mar. Geology*, *207*, 145–157, doi:10.1016/j.margeo.2004.04.002.

Grevemeyer, I., C. R. Ranero, E. Flueh, D. Kläschen, and J. Bialas (2007), Passive and active seismological study of bending-related faulting and mantle serpentinization at the Middle America trench, *Earth Planet. Sci Lett.*, *258*, 528–542, doi:10.1016/j.epsl.2007.04.013.

Han, X., E. Suess, H. Sahling, and K. Wallmann (2004), Fluid venting activity on the Costa Rica margin: New results from authigenic carbonates, *Int. J. Earth Sci. (Geol Rundsch)*, *93*, 596–611, doi 10.1007/s00531-004-0402-y.

Harris, R. N., I. Grevemeyer, C. R. Ranero, H. Villinger, U. Barckhausen, T. Henke, C. Mueller, and S. Neben (2010a), Thermal regime of the Costa Rican convergent margin: 1. Along-strike variations in heat flow from probe measurements and estimated from bottom-simulating reflectors, *Geochem. Geophys. Geosyst.*, *10*, doi:1029/2010GC003272.

Harris, R.N., G. Spinelli, C. R. Ranero, I. Grevemeyer, H. Villinger, and U. Barckhausen (2010b), Thermal regime of the Costa Rican convergent margin: 2. Thermal models of the shallow Middle America subduction zone offshore Costa Rica, *Geochem. Geophys. Geosyst.*, *11*, doi:1029/2010GC003273.

Heinio, P., and R. J. Davies (2009), Trails of depressions and sediment waves along submarine channels on the continental margin of Espirito Santo Basin, Brazil., *Bull. of the Geol. Soc. of Amer.*, *64* (11), 1295-1314, doi:10.1130/B26190.1.

Hensen, C., K. Wallmann, M. Schmidt, C. R. Ranero, and E. Suess (2004), Fluid expulsion related to mud extrusion off Costa Rica—A window to the subducting slab, *Geology*, *32*, 201-204, doi:10.1130/G20119.1.

Hovland, M., and A. G. Judd (1992), The global production of methane from shallow submarine sources, *Cont. Shelf Res.*, *12*, 1231-1238, doi:10.1130/ G20119.1.

Hovland, M., J. V. Gardner, and A. G. Judd (2002), The significance of pockmarks to understanding fluid flow processes and geohazards, *Geofluids*, *2*, 127-136, doi:10.1046/j.1468-8123.2002.00028.x.

Hutnak, M., et al. (2007), The thermal state of 18–24 Ma upper lithosphere subducting below the Nicoya Peninsula, northern Costa Rica margin, in The Seismogenic Zone of Subduction Thrust Faults, edited by T. Dixon, and C. Moore, Columbia Univ. Press, New York, 42–85.

Jobe, Z. R., D. R. Lowe, and S. J. Uchytil (2011), Two fundamentally different types of submarine canyons along the continental margin of Equatorial Guinea, *Mar. and Petro. Geol.*, *28*, 843–860, doi:10.1016/j.marpetgeo.2010.07.012.

Judd, A., and M. Hovland (2007), Seabed Fluid Flow, *Cambridge University Press*.

Karaca, D., C. Hensen, and K. Wallmann (2010), Controls on authigenic carbonate precipitation at cold seeps along the convergent margin off Costa Rica, *Geochem. Geophys. Geosys.*, *11*, Q08S27, doi:1029/2011GC003062.

Kahn, L. M., E. A. Silver, D. L. Orange, R. Kochevar, and B. G. McAdoo (1996), Surficial evidence of fluid expulsion from the Costa Rica accretionary prism, *Geophys. Res. Lett.*, *23*, 887-890.

Kimura, G., E. Silver, and P. Blum, (1997), (Eds) Proc. ODP, Init. Repts., *Ocean Drilling Program*, College Station, Texas.

Klaucke, I., D. G. Masson, C. J. Peterson, W. Weinrebe, and C. R. Ranero (2008), Multifrequency geoacoustic imaging of fluid escape structures offshore Costa Rica: Implications for the quantification of seep processes, *Geochem. Geophys. Geosyst.*, *9*, Q04010, doi:10.1029/2007GC001708.

Kluesner, J. W, and P. Lonsdale (2010), Large-scale pockmarks on the west margin of Baja California (abs), *Amer. Geophys. Un. Fall Meeing*, San Francisco, CA.

Kulm, L.D., E. Suess, J. C. Moore, et al. (1986), Oregon subduction zone: Venting, fauna, and carbonates, *Science*, *231*, 561-566.

Kvenvolden, K. A. (1993), Gas hydrates—Geological perspective and global change, *Rev. Geophys.*, *31*, 173-187.

Kvenvolden, K. A., and B. W. Rogers (2005), Gaia's breath—Global methane exhalations, *Mar. Petrol. Geol.*, *22*, 579-590, doi:10.1016/j.marpetgeo.2004.08.004.

Langseth, M. G., and E. A. Silver (1996), The Nicoya convergent margin—A region of exceptionally low heat flow, *Geophys. Res. Lett.*, *23*, 891–894.

Løseth, H., M. Gading, and L. Wensaas (2009), Hydrocarbon leakage interpreted on seismic data, *Mar. and Petrol. Geol.*, *26*, 1304–1319, doi:10.1016/j.marpetgeo.2008.09.008.

Mau, S., G. Rehder, I. G. Arroyo, J. Gossler, and E. Suess (2007), Indications of a link between seismotectonics and CH4 release from seeps off Costa Rica, *Geochem. Geophys. Geosyst.*, *8*, Q04003, doi:10.1029/2006GC001326.

Mau, S., G. Rehder, H. Sahling, T. Schleicher, and P. Linke (2012), Seepage of methane at Jaco Scar, a slide caused by seamount subduction offshore Costa Rica, *Int. J. Earth Sci.*, (Geol. Rundsch), doi:10.1007/s00531-012-0822-z.

McAdoo, B. G., D. L. Orange, E. A. Silver, K. D. McIntosh, L. D. Abbott, J. Galewsky, L. M. Kahn, and M. Protti (1996), Seafloor structural observations, Costa Rica accretionary prism, *Geophys. Res. Lett.*, *23*, 883–886.

McConnell, D. R., and B. A. Kendall (2003), Images of the base of gas hydrate stability in the deepwater Gulf of Mexico: Examples of gas hydrate traps in the northwest Walker Ridge and implications for successful well planning, *The Leading Edge*, *22*, 361-367, doi:10.1190/1.1572091.

McIntosh, K. D., and E. A. Silver (1996), Using 3D seismic reflection data to find fluid seeps from the Costa Rica accretionary prism, *Geophys. Res. Lett.*, *23*, 895-898.

Moore, J. C., and D. Saffer (2001), Updip limit of the seismogenic zone beneath the accretionary prism of southwest Japan: An effect of diagenetic to low-grade metamorphic processes and increasing effective stress, *Geology*, *29*, 183–186.

Morris, J. D., H. W. Villinger, A. Klaus, et al. (2003), Proc. ODP, Init. Repts., *Ocean Drilling Program*, 205, College Station, TX, doi:10.2973/odp.proc.ir.205.101.2003.

Newman, A. V., S. Y. Schwartz, V. Gonzalez, H. R. DeShon, J. M. Protti, and L. M. Dorman (2002), Along-strike variability in the seismogenic zone below Nicoya Peninsula, Costa Rica, *Geophys. Res. Lett.*, *29*, doi:10.1029/2002GL015409.

Orange, D. L., P. A. Teas, and J. Decker (2010), Multibeam backscatter—Insights into Marine Geological Processes and Hydrocarbon Seepage, *Offshore Technology Conference*, Houston, Texas, CD-ROM paper #20860.

Paull, C. K., W. III Ussler, W. S. Boroski, and F. N. Spiess (1995), Methane-rich plumes on the Carolina continental rise: Associations with gas hydrates, *Geology*, *23*, 89-92.

Peterson, C. J., I. Klaucke, W. Weinrebe, and C. R. Ranero (2009), Fluid seepage and mound formation offshore Costa Rica revealed by deep-towed sidescan sonar and sub-bottom profiler data, *Mar. Geol.*, *266*, 172-181, doi:10.1016/j.margeo.2009.08.004.

Pilcher, R., and J. Argent (2007), Mega-pockmarks and linear pockmark trains on the West African continental margin, *Mar. Geol.*, *244*, 15-32, doi:10.1016/j.margeo.2007.05.002.

Protti, M., et al. (1995), The March 25, 1990 (M_w=7.0, M_l=6.8), earthquake at the entrance of the Nicoya Gulf, Costa Rica: Its prior activity, foreshocks, aftershocks, and triggered seismicity, *J. Geophys. Res.*, *100*, 20,345-20,358.

Ranero, C. R., J. Phipps Morgan, K. McIntosh, and C. Reichert (2003), Bending-related faulting and mantle serpentinization at the Middle America Trench, *Nature*, *425*, 367-373, doi:10.1038/nature01961.

Ranero, C., I. Grevemeyer, Sahling, U. Barckhausen, C. Hensen, K. Wallmann, W. Weinrebe, P. Vannucchi, R. von Huene, and K. McIntosh (2008), Hydrogeological system of erosional convergent margins and its influence on tectonics and interplate seismogenesis, *Geochem. Geophys. Geosyst.*, *9*, Q03S04. doi:10.1029/2007GC001679.

Ranero, C. R., and R. von Huene (2000), Subduction erosion along the Middle America convergent margin, *Nature*, *404*, 748–752.

Ruppel, C., and M. Kinoshita (2000), Heat, fluid, and methane flux on the Costa Rican active margin off the Nicoya Peninsula, *Earth and Planet. Sci. Lett.*, *179*, 153-165.

Sahling, H., D. G. Masson, C. R. Ranero, V. Huhnerbach, W. Weinrebe, I. Klaucke, D. Burk, W. Bruckmann, and E. Suess (2008), Fluid seepage at the continental margin offshore Costa Rica and southern Nicaragua, *Geochem. Geophys. Geosyst.*, *9*, Q05S05, doi:10.1029/2008GC001978.

Siddall, M., E. Rohling, A. Almogi-Labin, C. Hemieben, D. Meischner, I. Schmelzer, and D. Smeed (2003), Sea-level fluctuations during the last glacial cycle, *Nature*, *423*, 853-858, doi:10.1038/nature01690.

Shipley, T. H., K. D. McIntosh, E. A. Silver, and P. L. Stoffa (1992), Three-dimensional seismic imaging of the Costa Rica accretionary prism: Structural diversity in the lower-slope, *J. Geophys. Res.*, *97*, 4439-4459.

Silver, E., M. Kastner, A. Fisher, J. Morris, K. McIntosh, and D. Saffer (2000), Fluid flow paths in the Middle America Trench and Costa Rica margin, *Geology*, *28*(8), 679–682, doi:10.1130/0091.

Solomon, E. A., M. Kastner, G. Wheat, H. W. Jannasch, G. Robertson, et al. (2009), Long-term hydrogeochemical records in the oceanic basement and forearc prism at the Costa Rica subduction zone. *Earth Planet. Sci. Lett.*, *282*, 240–51, doi:10.1016/j.epsl.2009.03.022.

Sitchler, J. C., D. M. Fisher, T. W. Gardner, and M. Protti (2007), Constraints on inner forearc deformation from balanced cross sections, Fila Costeña thrust belt, Costa Rica, *Tectonics*, *26*, TC6012, doi: 10.1029/2006TC001949.

Sun, Q., S. Wu, M. Hovland, P. Luo, Y. Lu, and T. Qu (2011), The morphologies and genesis of mega-pockmarks near the Xisha Uplift, South China Sea, *Mar. and Petr. Geol.*, *28*, 1146–1156, doi:10.1016/j.marpetgeo.2011.03.003.

Tryon, M. D., C. G. Wheat, and D. R. Hilton, (2010), Fluid sources and pathways of the Costa Rica erosional convergent margin, *Geochem. Geophys. Geosyst.*., *11*, doi:10.1029/2009GC002818.

Vannucchi, P., D. W. Scholl, M. Meschede, and K. McDougall-Reid (2001), Tectonic erosion and consequent collapse of the Pacific margin of Costa Rica: Combined implications from ODP Leg 170, seismic offshore data, and regional geology of the Nicoya Peninsula, *Tectonics*, *20*, 649-668.

Vannucchi, P., C. Ranero, S. Galeotti, S. M. Straub, D. W. Scholl, and K. McDougall-Reid (2003), Fast rates of subduction erosion along the Costa Rica Pacific margin: Implications for nonsteady rates of crustal recycling at subduction zones, *J. Geophys. Res.*, *108*, doi:10.1029/2002JB002207.

Vannucchi, P., and L. Leoni (2007), Structural characterization of the Costa Rica decollement: Evidence for seismically induced fluid pulsing, *Earth Planet. Sci. Lett.*, *262*, 413–428, doi:10.1016/j.epsl.2007.07.056.

Vannucchi, P., K. Ujiie, N. Stroncik, A. Malinverno, and the Expedition 334 Scientists, (2012), Site U1378. Proc. *International Ocean Drilling Program*, 334: Tokyo (IODP Management International, Inc.). doi:10.2204/iodp.proc.334.103.2012.

Van Rensbergen, P., A. Rabaute, A. Colpaert, T. St. Ghislain, M. Mathijs, and A. Bruggeman (2007), Fluid migration and fluid seepage in the Connemara Field, Porcupine Basin interpreted from industrial 3D seismic and well data combined with high-resolution site survey data, *Int. J. Earth Sci.*, *96*, 185–197.

von Huene, R., C. Ranero, W. Weinrebe, and K. Hinz (2000), Quaternary convergent margin tectonics of Costa Rica: Segmentation of the Cocos Plate and Central American volcanism, *Tectonics*, *19*, 314-334.

Ye, S., J. Bialas, E. R. Flueh, A. Stavenhagen, and R. von Huene (1996), Crustal Structure of the Middle American Trench off Costa Rica from wide-angle seismic data, *Tectonics*, *15*, 1006-1021.